Assessment of radiation shielding properties in borosilicate glasses doped with Er_2O_3

Selim KAYA[*1]

[1] *Department of Physics Engineering, Faculty of Engineering and Natural Sciences,* Gümüşhane University, Turkey

[*]*selimkaya@gumushane.edu.tr*

ATIF/REFERENCE: Kaya, S. (2024). Assessment of radiation shielding properties in borosilicate glasses doped with Er_2O_3. *International Journal of Advanced Natural Sciences and Engineering Researches*, 8(11), 1-12.

Abstract – This study systematically evaluated the gamma-ray shielding abilities of borosilicate glass samples with the chemical formula $70B_2O_3–5SiO_2–10Li_2O–5Bi_2O_3–10ZnO–XEr_2O_3$ and X = 0.0 (Er-0.0) to 1.2 (Er-1.2) mol% (abbreviated as BSLBZE). Using the EGS4 calculation code, shielding properties were determined for a total of 20 energies from 0.05 MeV to 2 MeV and then compared with data generated by XCOM. An increase in glass density from 2.95 g/cm³ to 3.12 g/cm³ was observed when the Er_2O_3 concentration was increased. A number of important radiation shielding parameters, such as gamma-ray kerma coefficients (kγ), radiation shielding efficiency (RPE), mean free path (MFP), fast neutron macroscopic cross section ΣR (cm^{-1}) and half-value layer (HVL), were determined. Samples with increased erbium doping have higher values for radiation protection efficiency (RPE), gamma-ray kerma coefficients (κ), and the fast neutron macroscopic cross-section ΣR (cm^{-1}), whereas the half-value layer (HVL) and mean free path (MFP) have lower values. The results demonstrate that increasing Er_2O_3 concentrations gradually improve the material's radiation shielding properties, with notable effectiveness in photon and neutron attenuation. This development significantly improves the glass matrix's overall shielding capabilities.

Keywords: Borosilicate glasses, Radiation protection efficiency, γ-kerma coefficient, EGS4

I. INTRODUCTION

In many scientific and practical fields, the way materials behave when exposed to gamma-ray radiation is crucial. Applications for gamma photons may be found in imaging, radiation, medical physics, space technology, and more. Radiation physicists and nuclear engineers are motivated to investigate more appropriate radiation shielding solutions by the growing prevalence of application in various sectors. Because of its penetration, gamma-ray photons are widely used in many different sectors, and their interaction with matter is a focus of study and development. Knowing how materials react to gamma-ray radiation is essential for designing shields, detection systems, and reducing background noise in high-energy particle physics investigations.

The concentration and ratio of Er_2O_3 to Bi_2O_3 determine how effective Er_2O_3-doped borate glasses are as radiation shields. Because of the glass's higher density and atomic number, increasing the concentration of Er_2O_3 leads to improved photon attenuation [1]. For use in laser and amplifier applications, high optical quality Er^{3+}-doped borate glasses have been created using a variety of manufacturing techniques.

These consist of the traditional sol-gel, sintering, and melt-quenching procedures [2]. Careful manufacturing process control is necessary to achieve a high density and uniform distribution of rare earth dopants without sacrificing optical quality in order to produce glass with the best shielding capacity [3]. It is commonly known that the radiation shielding properties of glass are significantly enhanced by the addition of heavy metals.

A crucial factor in comprehending how radiation and matter interact is the mass attenuation coefficient (MAC). Important in the fields of industry, medicine, and research, this coefficient quantitatively describes a material's capacity to reduce radiation as it travels through it. Among the radiation types used in medical imaging, including computed tomography (CT) scans and X-rays, different attenuation coefficients are observed when they interact with human tissues. These coefficients have a significant impact on the resolution and diagnostic accuracy of medical images, so a thorough understanding of them is essential. Thus, internal anatomical structures and possible clinical anomalies can be visualized more accurately. The creation of incredibly precise and therapeutically meaningful images is guaranteed by taking these factors into account when improving imaging methods.The field of radiation protection requires a thorough understanding of the mass attenuation coefficient (MAC) for different shielding materials. The design and implementation of efficient barriers to reduce radiation exposure in settings where radiation offers a serious concern, including nuclear power plants, hospitals, and industrial operations, are supported by this understanding. In order to maximize radiation attenuation and improve the effectiveness of safety procedures, engineers and radiation safety specialists use these coefficients to choose suitable materials and create structural solutions.

In industrial radiography, where radiation is used for non-destructive testing to find material faults or perform quality evaluations, the mass attenuation coefficient (MAC) is also very important. The MAC guarantees accurate material characterization and trustworthy fault diagnosis by making it easier to choose appropriate shielding materials and permitting accurate interpretation of radiography data. Thus, upholding high standards of analytical precision and quality assurance in industrial applications requires a detailed grasp of the attenuation properties of various compounds. In conclusion, researchers can gain important knowledge on the composition, structural qualities, and physical attributes of materials by examining the mass attenuation coefficient (MAC). Advances in a variety of fields, including as scientific research, safety engineering, medical imaging, and technology innovation, are fueled by this fundamental knowledge. The MAC's crucial function highlights how essential it is to promoting advancement and improving techniques across a wide range of industries.

The development of radiation-resistant materials requires an understanding of how materials behave under gamma-ray radiation. When designing and optimizing materials that can withstand the extreme radiation environments found in high-energy particle physics experiments, critical parameters such as the mass attenuation coefficient (MAC), radiation protection efficiency (RPE), and gamma-ray kerma coefficient (kγ) are essential. For improving material performance and resilience in such demanding applications, these characteristics offer a scientific foundation [4].

The Radiation Protection Efficiency (RPE) measures how well a substance protects against radiation exposure. Fast neutron removal cross sections show how long a neutron is subjected to a certain kind of transmission (such absorption or scattering) in a given material per unit route length. Furthermore, the energy that gamma-ray photons impart to the material through different interactions is evaluated by the Gamma-ray Kerma Coefficient (kγ).

In order to determine the mass attenuation coefficients and photon cross sections for elements, compounds, and combinations across a broad range of energies, from 1 keV to 100 GeV, Berger and Hubbell created the XCOM software. [5]. In order to improve the software's usability and accessibility, Gerward et al. created WinXCOM, a modified version of XCOM. [6]. Monte Carlo simulation methods were used to establish the mass attenuation coefficients and other crucial factors necessary for comprehending gamma-ray interactions. By precisely simulating the stochastic behavior of gamma rays as they pass through different materials, these computational techniques offer comprehensive insights into the mechanisms of attenuation and interaction. [7-12].

In this study, the mass attenuation coefficients of glasses doped with Er_2O_3 were theoretically Monte Carlo EGS4 and winXCOM calculated energies from 0,05 MeV to 2 MeV. The theoretically calculated mass attenuation coefficient (MAC) values from XCOM and EGS4 were employed to derive several shielding parameters, including the mean free path (MFP), half-value layer (HVL), radiation protection efficiency (RPE), fast neutron macroscopic cross-section ΣR (cm^{-1}) and gamma kerma coefficients ($k\gamma$).

II. MATERIALS AND METHOD

Monte Carlo Simulation

In the present investigation, EGS4 (Electron Gamma Showers) Nelson and Hirayama was utilized to calculate kerma coefficients and gamma attenuation parameters [13]. To model the HPGe detector response, Monte Carlo simulations were performed using the EGS4. Using a certified random number generator is essential for MC calculations since random number production is crucial. The EGS4 code was implemented using a RANLUX random number generator, which has been demonstrated to generate a longer sequence and a comparatively superior distribution [14]. 10,010 energy bins with a width of 0.3 keV each were created from the efficiency for the model run using EGS4. After dividing the computed area into 241 cells, the form is rotated 360 degrees on the -axis shown in **Fig.** 1 to produce a cylindrical geometry. Assumedly, Fig. 1 depicts a sequence of cylindrical circular projectiles, each having a plane denoted by P1, P2, …., P20, and a radius denoted by R1, R2, …, R11. For the point radioactive source, a section of code was written such that all photons were emitted along the z-axis, producing a beam of collimated photons. [8,9,15].
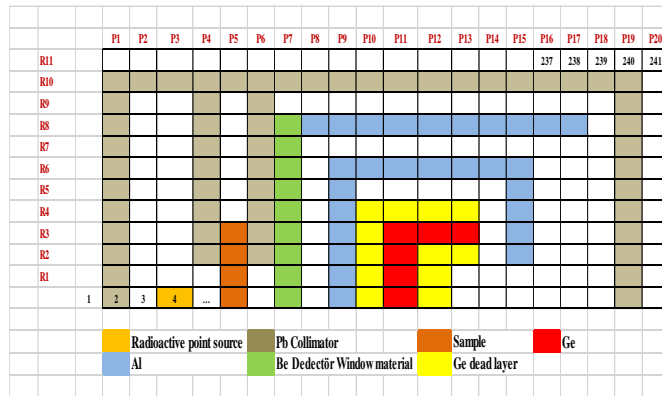
Fig. 1. Detector model for Monte Carlo (ESG4 code) calculations.

Gamma attenuation parameters

In this study, the mass attenuation coefficients (MAC) parameters of samples were determined as follows. The attenuation of gamma rays in a material can be described using the Beer-Lambert law, which states:

$$I = I_0 e^{-\mu x} \qquad (1)$$

where *I* is the intensity of the gamma-ray beam after it has passed through a thickness x of the material, I_0 is the initial intensity of the beam and μ (cm^{-1}) is the linear attenuation coefficient of the material for the specific energy of the gamma rays being considered.

While the linear attenuation coefficient (μ) is commonly used to describe how strongly a material absorbs gamma rays, it has the disadvantage of depending on the density of the material. Therefore, it is often more useful to use the density-independent mass attenuation coefficient (μ/ρ), which is expressed in units of cm^2/g. The density-independent mass attenuation coefficient can be calculated using the following formula μ/ρ (cm^2/g):

$$I = I_0 e^{-(\mu/\rho)\rho x} = I_0 e^{-(\mu/\rho)d} \qquad (2)$$

According to the Beer-Lambert law equation, the thickness "d" is expressed in unit area mass of the material (g/cm^2). When a sample contains more than one metal, the mass attenuation coefficient (μ/ρ) of the sample can be calculated using the mixture rule formula, which is given as:

$$\mu/\rho = \sum_i w_i (\mu/\rho)_i \qquad (3)$$

where w_i is the weight fraction of the ith component in the sample and $(\mu/\rho)_i$ is the density-independent mass attenuation coefficient of the ith component [16].

The weight fraction (wi) of a chemical component i in a mixture can be calculated using the following relation:

$$w_i = \frac{a_i A_i}{\sum a_i A_i} \qquad (4)$$

where a_i is the number of formula units, Ai is the atomic weight of the ith element, and the summation is taken over all components in the mixture. Mass attenuation coefficients (μ $\rho/$) of the samples under study are computed by Monte Carlo-EGS4 simulation code and compared to WinXCOM results in the energy range 0.05–2 MeV.

The theoretical mass attenuation coefficients (μ/ρ) of samples were determined using WinXCom software [6,8,17,18].

Half value layer (HVL) of the materials is the thickness that reduced the half of the radiation entering it [19]: The HVL can be calculated using the following equation

$$HVL = ln2/\mu \qquad (6)$$

The mean free path (MFP) is a measure of the average distance a particle or photon can travel in a material before it interacts with the material in some way, such as absorption, scattering, or transmission. In general, the MFP is the inverse of the linear attenuation coefficient (μ) of a material, which describes how much radiation is absorbed or scattered per unit length of the material. The mean free path (MFP) were calculated using μ values as follows [20]:

$$MFP = 1/\mu \qquad (8)$$

where, μ is the linear attenuation coefficient, whose unit of measurement is cm^{-1}.

The radiation protection efficiency (RPE) parameter of sampless was investigated. The efficiency (RPE) in terms from incoming and transmitted photon densities is given equation below [21]:

$$RPE = \left(1 - \frac{I}{I_0}\right) * 100 \qquad (9)$$

Kerma coefficient (Gy.cm^2/photon) for uncharged particles can be calculated using the mass attenuation coefficient and partial interaction probabilities. It is given by the equation:

$$K = k\phi\left[\frac{\mu_{tr}}{\rho}\right] \qquad (10)$$

where K is uncharged radiation of energy E, $k\phi$ is the kerma coefficient and μ_{tr}/ρ is the mass energy-transfer coefficient of the substance [22].
Methods for finding the photon kerma coefficients of samples have been given in previous studies [8,11,23,24].

A key metric in nuclear reactor analysis and neutron transport theory is the fast neutron macroscopic cross-section ΣR (cm−1), which captures the interaction probability per unit distance traveled by fast neutrons in a material medium. The following relationship is used to get the ΣR value for neutron shielding materials.

$$\Sigma_R / \rho = \sum_i w_i (\Sigma_R/\rho)_i \qquad (11)$$

and

$$\Sigma_R = \sum_i \rho_i (\Sigma_R/\rho)_i \qquad (12)$$

where the partial density of the ith element is represented by ρi (g/cm^3) and the fast neutron removal cross section by ΣR/ρ (cm^2/g) [19,25,27]. The following formula can be used to determine the partial density of the i-th element, represented as (ρi):

$$\rho_i = \rho \times w_i \qquad (13)$$

Here, wi stands for the weight fraction of the ith element, and ρ for the sample's density (g/cm³). [19].

III. RESULTS AND DISCUSSION

The present study evaluated the effect of varying Er_2O_3 concentrations on the radiation shielding effectiveness of $70B_2O_3–5SiO_2–10Li_2O–5Bi_2O_3–10ZnO–XEr_2O_3$ glass composition using x values of 0, 0.3, 0.6, 0.9, and 1.2 mol%. $70B_2O_3–5SiO_2–10Li_2O–5Bi_2O_3–10ZnO–XEr_2O_3$ with X = 0.0, 0.3, 0.6, 0.9, and 1.2 mol% glasses were prepared by the melt quenching technique method [28].

Chemical composition of BSLBZE glasses system doped with Er_2O_3 (% weight percentage) is given **Table 1.** Calculated EGS4 and XCOM mass attenuation coefficients μ/ρ (cm² g⁻¹), samples at different 20 energies from 0.05 to 2 MeV have been given in **Table 2.** Theoretical (K_T) and simulation (K_{EGS4}) kerma coefficients for the samples have been given in **Table 3.** The variation of the mass attenuation coefficients with the energy for samples is given **Fig 2.** borosilicate glasses doped with Er_2O_3 change graph of HVL and MFP values versus photon energy. Variation of energy with half value layer (HVL) and mean free path (MFP) for given samples was plotted in the 1 keV–100 MeV energy range and shown in **Fig 3 and 4**, respectively. As photon energy increases, it can be observed from these figures that the Half Value Layer (HVL) and Mean Free Path (MFP) values for the samples under investigation both rise.

Fig. 5 shows changes of RPE with photon energy for investigated samples. In figure 5, it is seen that the RPE values decrease as the photon energy increases.

The different samples ΣR were computed and shown in **Fig 6.** As seen in Figure 6, BSLBZE-5 has the largest ΣR (cm⁻¹) value compared to other samples. It is therefore the most effective material for absorbing neutrons and offers superior defence against gamma radiation.

The graph of change of gamma kerma coefficients for Borosilicate glass samples doped with Er_2O_3 is shown in **Fig. 7**. In the mid-energy spectral domain, as photon energy ascends, the relative prominence of Compton scattering and pair production escalates vis-a-vis the photoelectric interaction, which in turn precipitates a diminution in the kerma coefficient.

The characteristics of the kerma coefficient curves vs. gamma-ray energy depend on the relative dominance of numerous photon interaction mechanisms, including the photoelectric effect, Compton scattering, and pair creation.

The relative contributions of each of these interaction modes depend on the photon energy and the atomic number of the material absorbed. Because Compton scattering and pair creation become more important in relation to the photoelectric interaction, the kerma coefficient drops as photon energy increases in the intermediate energy range.

Table 1. Chemical composition of BSLBZE glasses system doped with Er_2O_3 (% weight percentage)

BSLBZE glasses system	Density ρ (g/cm³)	Li	B	O	Si	Zn	Er	Bi

doped with Er_2O_3

BSLBZE-1	2.95	1.61	17.57	47.35	1.63	7.59	0.00	24.25
BSLBZE-2	2.99	1.59	17.34	46.89	1.61	7.49	1.15	23.94
BSLBZE-3	3.03	1.57	17.11	46.45	1.59	7.39	2.27	23.62
BSLBZE-4	3.08	1.55	16.89	46.01	1.57	7.30	3.36	23.32
BSLBZE-5	3.12	1.53	16.68	45.59	1.55	7.21	4.42	23.03

Table 2. Calculated (EGS4) and Theoretical (XCOM) values of mass attenuation coefficients μ/ρ (cm^2/g)

Energy (keV)	Mass attenuation coefficients μ/ρ (cm^2/g)									
	Sample-1		Sample-2		Sample-3		Sample-4		Sample-5	
	XCOM	EGS4	XCOM	EGS4	XCOM	EGS4	XCOM	EGS4	XCOM	EGS4
50	2.391	2.407	2.414	2.417	2.435	2.418	2.456	2.467	2.477	2.466
59.54	1.560	1.528	1.699	1.692	1.835	1.828	1.968	1.948	2.097	2.107
80	0.786	0.776	0.851	0.840	0.913	0.909	0.975	0.989	1.034	1.054
100	1.532	1.540	1.554	1.528	1.575	1.557	1.596	1.582	1.616	1.621
122	0.966	0.963	0.979	0.964	0.991	0.961	1.003	0.994	1.014	1.017
150	0.613	0.611	0.620	0.611	0.627	0.632	0.634	0.633	0.640	0.645
200	0.345	0.347	0.348	0.352	0.351	0.365	0.354	0.364	0.357	0.371
300	0.181	0.184	0.182	0.180	0.183	0.177	0.184	0.183	0.184	0.189
383	0.135	0.141	0.135	0.139	0.136	0.134	0.136	0.140	0.137	0.144
400	0.129	0.123	0.129	0.124	0.130	0.135	0.130	0.135	0.130	0.133
511	0.103	0.109	0.103	0.107	0.103	0.106	0.103	0.096	0.103	0.098
600	0.091	0.095	0.091	0.094	0.091	0.095	0.091	0.093	0.091	0.092
662	0.084	0.085	0.084	0.087	0.084	0.085	0.085	0.089	0.085	0.088
800	0.074	0.079	0.074	0.073	0.074	0.072	0.074	0.079	0.074	0.078
1000	0.064	0.061	0.064	0.063	0.064	0.068	0.064	0.061	0.064	0.062
1173	0.059	0.056	0.059	0.059	0.058	0.062	0.058	0.054	0.058	0.058
1274	0.056	0.055	0.056	0.054	0.056	0.055	0.056	0.052	0.056	0.057
1332	0.054	0.053	0.054	0.052	0.054	0.054	0.054	0.049	0.054	0.052
1500	0.051	0.049	0.051	0.050	0.051	0.051	0.051	0.047	0.051	0.050
2000	0.044	0.045	0.044	0.042	0.044	0.043	0.044	0.044	0.044	0.045

Table 3. Calculated (EGS4) and Theoretical (XCOM) values of kerma coefficients *k* (in pGy.cm2/photon)

Energy (keV)	Kerma coefficients *k* (in pGy.cm2/photon)									
	Sample-1		Sample-2		Sample-3		Sample-4		Sample-5	
	XCOM	EGS4	XCOM	EGS4	XCOM	EGS4	XCOM	EGS4	XCOM	EGS4
50	16.619	16.728	16.774	16.798	16.925	16.806	17.071	17.147	17.215	17.140
59.54	12.309	12.068	13.620	13.572	14.897	14.848	16.141	15.990	17.353	17.449
80	7.425	7.328	8.234	8.131	9.023	8.979	9.791	9.936	10.540	10.743
100	21.776	21.885	22.112	21.741	22.440	22.179	22.760	22.560	23.072	23.140
122	15.981	15.925	16.215	15.969	16.443	15.945	16.665	16.517	16.882	16.924
150	11.665	11.620	11.824	11.647	11.978	12.073	12.129	12.118	12.276	12.372
200	7.706	7.746	7.799	7.883	7.889	8.199	7.977	8.200	8.062	8.381
300	4.868	4.952	4.912	4.862	4.954	4.798	4.995	4.978	5.035	5.158
383	4.142	4.328	4.170	4.281	4.196	4.140	4.222	4.339	4.247	4.476
400	4.068	3.880	4.093	3.924	4.118	4.286	4.141	4.298	4.165	4.247
511	3.892	4.127	3.908	4.061	3.923	4.032	3.938	3.660	3.952	3.744
600	3.963	4.157	3.974	4.121	3.985	4.172	3.996	4.092	4.006	4.055
662	4.069	4.100	4.078	4.203	4.086	4.113	4.095	4.313	4.103	4.270
800	4.376	4.661	4.381	4.312	4.387	4.257	4.392	4.676	4.397	4.622
1000	4.901	4.639	4.904	4.795	4.906	5.179	4.908	4.649	4.911	4.729
1173	5.369	5.137	5.369	5.415	5.370	5.693	5.370	4.961	5.371	5.331
1274	5.641	5.561	5.641	5.462	5.623	5.566	5.623	5.264	5.622	5.773
1332	5.798	5.648	5.798	5.543	5.797	5.759	5.796	5.227	5.796	5.550
1500	6.257	6.009	6.256	6.134	6.254	6.258	6.253	5.769	6.252	6.139
2000	7.652	7.791	7.651	7.273	7.650	7.447	7.650	7.622	7.649	7.623
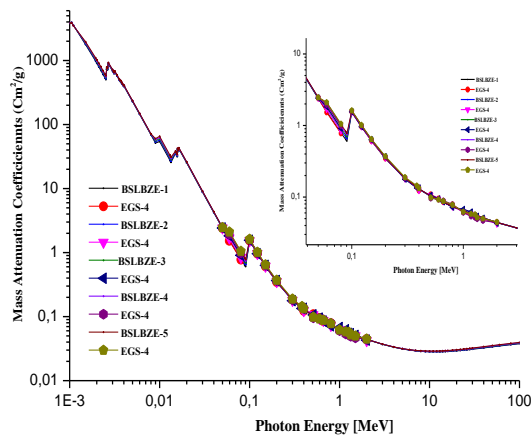
Fig. 2. The variation of the mass attenuation coefficients with the energy for samples.
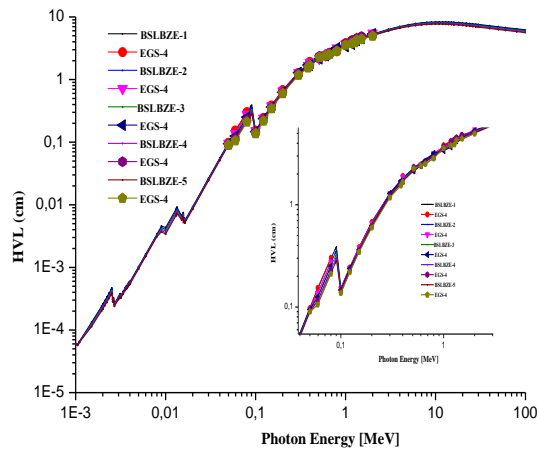
Fig. 3. The variation of the half value layer (HVL) with the energy for glasses doped with Er_2O_3
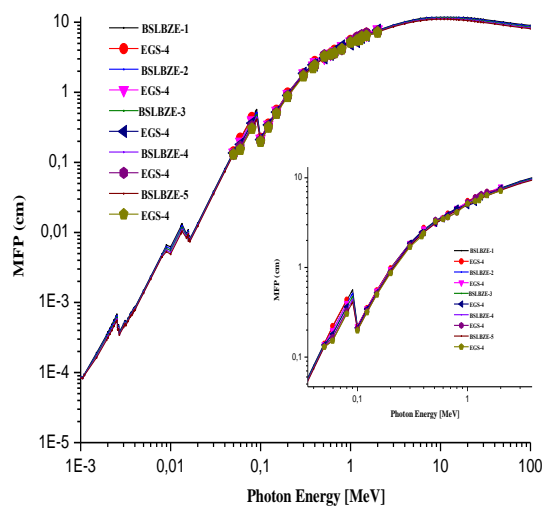
Fig. 4. The variation of the mean free path (MFP) with the energy for glasses doped with Er_2O_3
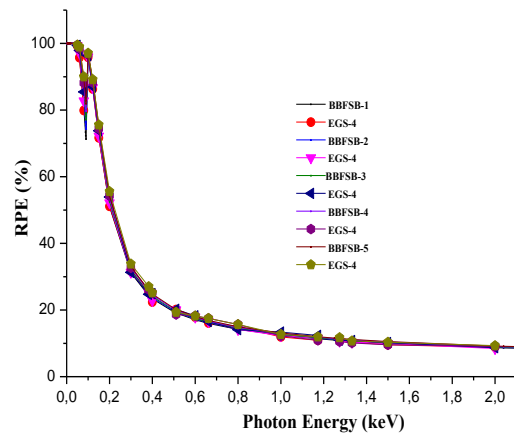
Fig. 5. The variation of radiation protection efficiency (RPE) of samples versus the photon energy
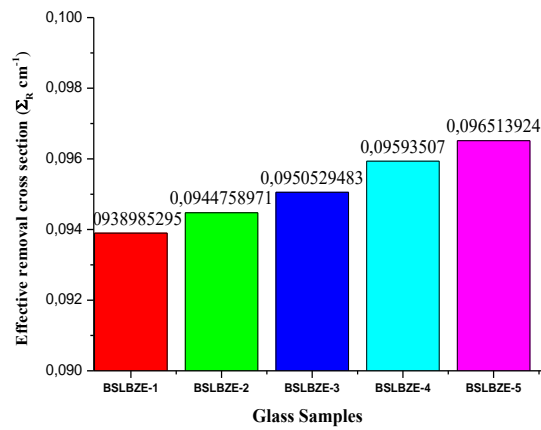
Fig. 6. Fast neutron macroscopic cross-section ΣR (cm^{-1}) of the given glass samples
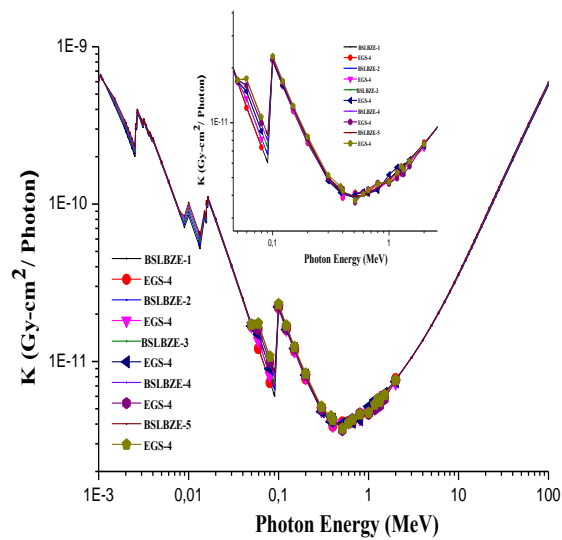
Fig. 7. The gamma kerma coefficients of samples as a function of photon energy

IV. CONCLUSION

This study seeks to investigate the influence of stoichiometric modifications in glasses doped with Er_2O_3 on radiation shielding parameters at gamma-ray energies from 0.05 to 2 MeV. Mass attenuation coefficients (μ/ρ) for glasses doped with Er_2O_3 were investigated theoretically (WinXCOM and EGS4).

it was determined some shielding parameters such as mean free path (MFP), half value layer (HVL), radiation protection efficiency (RPE), fast neutron macroscopic cross-section ΣR (cm−1) and gamma–ray kerma coefficients ($k\gamma$). As the density of Er_2O_3 doped glasses increases, a significant decrease in mass attenuation coefficients is observed, especially up to the first 500 keV. A decrease in the mean free path (MFP) in the half-value layer (HVL) at a fixed energy level for Er2O3 doped glass samples resulted in a significant increase in radiation shielding efficiency (RPE), fast neutron macroscopic cross-section ΣR (cm−1) and gamma-ray kerma coefficients.

The findings demonstrated that the most stable and efficient glass sample for shielding against X-ray and gamma radiation across all photon energy ranges is $70B_2O_3–5SiO_2–10Li_2O–5Bi_2O_3–10ZnO–1.2Er_2O_3$ (BSLBZE-5). Researching how materials respond to radiation, especially gamma rays and neutrons, is essential in a wide range of fields. Effective shielding materials are essential in nuclear power plants, medical imaging, space exploration, and even everyday applications where radiation exposure must be kept to a minimum. By understanding how various materials respond to radiation and attenuate it, researchers can develop better shielding materials.

To develop shielding solutions that are lighter, more durable, and more reasonably priced, this calls for not just improving shielding capabilities but also making efficient use of materials. It is vital to evaluate radiation shielding parameters in glass samples to improve safety procedures, improve material quality, and support advances in radiation shielding technologies. In addition to demonstrating exceptional efficacy and safety, this research will help design and develop glass systems with new properties specifically suited to meet the needs of high radiation exposure environments.

REFERENCES

[1] Acikgoz, A., Demircan, G., Yılmaz, D., Aktas, B., Yalcin, S., & Yorulmaz, N. (2022). Structural, mechanical, radiation shielding properties and albedo parameters of alumina borate glasses: Role of CeO2 and Er2O3. Materials Science and Engineering: B, 276, 115519.

[2] Wu, R., Du, P., Weng, W., & Han, G. (2006). Preparations and dielectric properties of Ba0. 80Sr0. 20TiO3/PbO–B2O3 thick films. Materials chemistry and physics, 97(1), 151-155.

[3] Kavaz, E., Ekinci, N., Tekin, H. O., Sayyed, M. I., Aygün, B., & Perişanoğlu, U. F. U. K. (2019). Estimation of gamma radiation shielding qualification of newly developed glasses by using WinXCOM and MCNPX code. Progress in nuclear energy, 115, 12-20.

[4] Baltaş, H., Çelik, Ş., Çevik, U., Yanmaz, E., 2007. Measurement of mass attenuation coefficients and effective atomic numbers for MgB2 superconductor using X-ray energies. Radiat. Meas. 42, 55–60.

[5] Berger, M. J., & Hubbell, J. H. (1999). XCOM: Photon cross-sections on a personnel computer (version 1.2). *NBSIR85-3597, National Bureau of Standarts, Gaithersburg, MD, USA, for version*, *3*.

[6] Gerward, L., Guilbert, N., Jensen, K.B., Levring, H., 2001. X-ray absorption in matter. Reengineering XCOM. Radiat. Phys. Chem. 60, 23–24.

[7] Tekin, H.O., Singh, V.P., Manici, T., 2017. Effects of micro-sized and nano-sized WO 3 on mass attenauation coefficients of concrete by using MCNPX code. Appl. Radiat. Isot. 121, 122–125.

[8] Baltas, H. (2020). Evaluation of gamma attenuation parameters and kerma coefficients of YBaCuO and BiPbSrCaCuO superconductors using EGS4 code. Radiation Physics and Chemistry, 166, 108517.

[9] Kaya, S., Çelik, N., and Bayram, T. (2022). Effect of front, lateral and back dead layer thicknesses of a HPGe detector on full energy peak efficiency. Nuclear Instruments and Methods in Physics Research Section A: Accelerators, Spectrometers, Detectors and Associated Equipment, 1029, 166401.

[10] El-Khayatt, A.M., Vega-Carrillo, H.R., 2015. Photon and neutron kerma coefficients for polymer gel dosimeters. Nucl. Instruments Methods Phys. Res. Sect. A Accel. Spectrometers, Detect. Assoc. Equip. 792, 6–10.

[11] El-Khayatt, A.M., 2017. Semi-empirical determination of gamma-ray kerma coefficients for materials of shielding and dosimetry from mass attenuation coefficients. Prog. Nucl. Energy 98, 277–284.

[12] Kaya, S., Çelik, N., Gök, A., & Çevik, U. (2023). Effect of detector crystal size on Compton suppression factors. Radiation Effects and Defects in Solids, 178(11-12), 1449-1462.

[13] Nelson, W.R., Rogers, D.W.O., Hirayama, H., 1985. The EGS4 code system.

[14] *Gasparro, J., Hult, M., Johnston, P.N., Tagziria, H., 2008. Monte Carlo modelling of germanium crystals that are tilted and have rounded front edges. Nucl. Instruments Methods Phys. Res. Sect. A Accel. Spectrometers, Detect. Assoc. Equip. 594, 196–201*

[15] Kaya, S. (2023). Calculation of the effects of silver (Ag) dopant on radiation shielding efficiency of BiPbSrCaCuO superconductor ceramics using EGS4 code. *Applied Sciences*, *13*(14), 8358.

[16] Kumar, A., Gaikwad, D.K., Obaid, S.S., Tekin, H.O., Agar, O., Sayyed, M.I., 2020. Experimental studies and Monte Carlo simulations on gamma ray shielding competence of (30+ x) PbO10WO3 10Na2O− 10MgO–(40-x) B2O3 glasses. Prog. Nucl. Energy 119, 103047

[17] Celik, N., Cevik, U., 2010. Monte Carlo determination of water concentration effect on gamma-ray detection efficiency in soil samples. Appl. Radiat. Isot. 68, 1150–1153

[18] *Gerward, L., Guilbert, N., Jensen, K.B., Leving, H., 2004. WinXCom–a program for calculating X-ray attenuation coefficients. Radiat. Phys. Chem. 71, 653–654*

[19] Tekin, H.O., Altunsoy, E.E., Kavaz, E., Sayyed, M.I., Agar, O., Kamislioglu, M., 2019. Photon and neutron shielding performance of boron phosphate glasses for diagnostic radiology facilities. Results Phys. 12, 1457–1464.

[20] Gaikwad, D.K., Sayyed, M.I., Botewad, S.N., Obaid, S.S., Khattari, Z.Y., Gawai, U.P., Afaneh, F., Shirshat, M.D., Pawar, P.P., 2019. Physical, structural, optical investigation and shielding featuresof tungsten bismuth tellurite-based glasses. J. Non. Cryst. Solids 503, 158–168.

[21] Sayyed, M. I., Akman, F., Kumar, A., & Kaçal, M. R. (2018). Evaluation of radioprotection properties of some selected ceramic samples.Results in Physics, 11, 1100-1104.

[22] Thomas, D.J., 2012. ICRU report 85: fundamental quantities and units for ionizing radiation.

[23] Attix, F.H., 2008. Introduction to Radiological Physics and Radiation Domisetry, John Wiley & Sons, U.S.A.

[24] Abdel-Rahman, W., Podgorsak, E.B., 2010. Energy transfer and energy absorption in photon interactions with matter revisited: A step-by-step illustrated approach. Radiat. Phys. Chem.

[25] El-Agawany, F. I., Kavaz, E., Perişanoğlu, U., Al-Buriahi, M., & Rammah, Y. S. (2019). Sm 2 O 3 effects on mass stopping power/projected range and nuclear shielding characteristics of TeO 2–ZnO glass systems. Applied Physics A, 125, 1-12.

[26] Yılmaz, E., Baltas, H., Kırıs, E., Ustabas, I., Cevik, U., El-Khayatt, A.M., 2011. Gamma ray and neutron shielding properties of some concrete materials. Ann. Nucl. Energy 38, 2204–2212.

[27] Sirin, M. (2020). The effect of titanium (Ti) additive on radiation shielding efficiency of Al25Zn alloy. Progress in nuclear energy, 128, 103470.

[28] Almuqrin, A., Al-Otaibi, J. S., Alwadai, N., Albarzan, B., Elsad, R. A., Shams, M. S., & Rammah, Y. S. (2024). Borosilicate glasses doped with Er2O3: preparation, physical, optical, dielectric properties and radiation shielding capacity. Applied Physics A, 130(12), 1-12.